LA-UR-15-27791 (Accepted Manuscript)

The Near-Earth Injection of MeV Electrons associated with Intense Dipolarization Electric Fields: Van Allen Probes observations

Dai, L.; Wang, C.; Duan, S.; He, Z.; Wygant, J.; Bonnell, J.; Cattell, C; Kletzing, C; Baker, D.; Funsten, Herbert O.; Reeves, Geoffrey D.

To be published in: Geophysical Research Letters (2015) Vol.42, iss.15, p.6170-6179, Aug 16 2015

DOI to publisher's version: 10.1002/2015GL064955

Permalink to record: http://permalink.lanl.gov/object/view?what=info:lanl-repo/lareport/LA-UR-15-27791

Near-Earth Injection of MeV Electrons associated with Intense Dipolarization Electric Fields: Van Allen Probes observations

Lei Dai[1,2], Chi Wang[1], Suping Duan[1], Zhaohai He[1], John R. Wygant[2], Cynthia A. Cattell[2], Xin Tao[3], Zhenpeng Su[3], Craig Kletzing[4], Daniel N. Baker[5], Xinlin Li[5], David Malaspina[5], J. Bernard Blake[6], Joseph Fennell[6], Seth Claudepierre[6], Drew L. Turner[6], Geoffrey D. Reeves[7], Herbert O. Funsten[7], Harlan E. Spence[8], Vassilis Angelopoulos[9], Dennis Fruehauff[10], Lunjin Chen[11], Scott Thaller[2], Aaron Breneman[2], Xiangwei Tang[2]

[1]State Key Laboratory of Space Weather,

Substorms generally inject 10s-100s keV electrons, but intense substorm electric fields have been shown to inject MeV electrons as well. An intriguing question is whether such MeV electron injections can populate the outer radiation belt. Here we present observations of a substorm injection of MeV electrons into the inner magnetosphere. In the pre-midnight sector at L$\sim$5.5, Van Allen Probes (RBSP)-A observed a large dipolarization electric field (50mV/m) over $\sim$40s and a dispersionless injection of electrons up to $\sim$3 MeV. Pitch angle observations indicated betatron acceleration of MeV electrons at the dipolarization front. Corresponding signals of MeV electron injection were observed at LANL-GEO, THEMIS-D, and GOES at geosynchronous altitude. Through a series of dipolarizations, the injections increased the MeV electron phase space density by one order of magnitude in less than 3 hours in the outer radiation belt (L>4.8). Our observations provide evidence that deep injections can supply significant MeV electrons.

National Space Science Center, Chinese

1. Introduction

Substorm dipolarization is known to inject energetic electrons into the radiation belts. Injected electrons are usually in the energy range from tens keV to hundreds keV. Observations and model results from the last two decades, however, indicate that dipolarizations sometimes inject MeV electrons, as well. In test particle simulations, *Kim et al.* [2000] showed that dipolarizations can contribute to MeV electrons enhancements in the outer radiation belt. *Ingraham et al.* [2001] provided observational evidence that strong substorms continuously inject MeV electrons to the geosynchronous altitude. Using data from the Akebono spacecraft, *Nagai et al.* [2006] identified rapid enhancements of MeV electrons associated with storm-time substorm dipolarizations in the outer radiation belt. Modeling results from *Fok et al.* [2001] and *Glocer et al.* [2011] attributed rapid enhancements of MeV electrons in their modeling results to dipolarization electric fields. Using data from multiple spacecraft that tracked the electron phase space density (PSD) at different radial locations, *Dai et al.* [2014] showed that strong dipolarization electric fields injected MeV electrons by pushing magnetotail electrons to the geosynchronous altitude. *Su et al.* [2014] provided evidence from the Van Allen Probes (RBSP) measurements that substorm injections of MeV electrons, as well as acceleration by chorus waves, contribute to the outward extension of the outer belt.

Substorm injections of MeV electrons are interesting from several perspectives. Their contribution to the energization of MeV electron in the radiation belt is relatively under-

Academy of Sciences, Beijing, China.

explored. The efficiency of this energization under different solar wind conditions and various levels of geomagnetic activity is unclear. Much of the physics of MeV electron injection remains to be explored. It now appears that only a small portion of substorm dipolarizations can inject MeV electrons. The special conditions under which substorm dipolarizations can inject MeV electrons are unknown. Furthermore, injections have been considered to provide the seed population needed for the local energization through wave-particle interactions. Injections of MeV electrons provide a harder spectrum of seed populations than injections of 10-100s keV electrons.

The electric field associated with dipolarizations, in which magnetic field lines collapse from a tail-like shape to a more dipole-like shape [*Baker et al.*, 1996], is believed to drive particle acceleration and injections [*Birn et al.*, 2013]. In observations, dipolarization electric fields are time-varying, azimuthally localized, and can be from mV/m to tens of mV/m [e.g.,*Cattell and Mozer* [1984]; *Fairfield et al.* [1998]; *Tu et al.* [2000]; *Dai et al.* [2014]]. Inspired by the injection front model [*Moore et al.*, 1981], *Li et al.* [1998] constructed a model of an earthward propagating electric field pulse to simulate the substorm injection. In the model of *Li et al.* [1998], the electric field pulse is associated with a rapid increase in $\mathbf{B}$z to represent the dipolarization. The model can produce signals of injections at different radial distances [*Li et al.*, 1998; *Sarris et al.*, 2002; *Li et al.*, 2003; *Zaharia et al.*, 2004; *Liu et al.*, 2009]. *Gabrielse et al.* [2012] developed a similar model, adding the

[2]School of Physics and Astronomy,

ingredient of twin vortices and their dawnward electric fields that are adjacent to the edge of the earthward flow. Alternative approaches to model the electric field and plasma dynamics of substorm dipolarizations involve MHD simulations [*Birn et al.*, 1998; *Fok et al.*, 2006; *Birn et al.*, 2013; *Ashour-Abdalla et al.*, 2011] and Rice Convection Model(RCM)-based simulations [*Zhang et al.*, 2009; *Yang et al.*, 2011].

Injected particles are trapped on closed orbits as the dipolarization electric field is reduced or diminished. As a result, deep injections can directly supply energetic particles to the center of the outer radiation belt. Using the CRRES data set, *Friedel et al.* [1996] showed that injections can penetrate to L=4. Such near-Earth injection events are also manifested as penetrating electric fields [*Rowland*, 2002]. *Sergeev et al.* [1998] documented short-duration injections that correlate with dawn-dusk electric fields at a radial distance of ∼5Re. In a study of multiple events, *Reeves et al.* [1996] showed that the injection region traveled earthward at an average of 24km/s from the geosynchronous altitude to the CRRES satellite. *Turner et al.* [2015] provided evidence of substorm-associated injections observed down to L = 2.5.

The orbit of Van Allen Probes (RBSP) [*Mauk et al.*, 2012] is suitable for studying near-Earth injections. To better understand MeV electron injections in the RBSP data set, we need to investigate the spatial scales of the injection region, the properties of the electric fields and magnetic fields, the characteristics of MeV electrons, and how many MeV elec-

University of Minnesota, Minneapolis, MN,

trons are injected during the dipolarizations. In this paper, we present detailed field and particle observations from RBSP, THEMIS, LANL-GEO and GOES of a MeV electron injection event in the inner magnetosphere. Previous observations of MeV electron injections has one limitation– only dispersionless injections were observed. In this study, we provide an unambiguous injection signature of the dispersed and drifting electron population up to $\sim$ 3MeV. This event is notable because of an extremely large dipolarization electric field 50mV/m that is rarely seen in previous models and observations.

2. Observations of Near-Earth Injection of MeV electrons

2.1. Overview of RBSP-A observations on 26 April 2013

With its apogee near midnight, RBSP-A spent several hours at L=5-6 in the nightside on 26 April, 2013. RBSP-B is not in an ideal orbit location to be relevant for this study. Figure 1 shows solar wind conditions, geomagnetic conditions and an overview of fields and energetic particles from RBSP-A from 03UT to 09UT on 26 April, 2013. As shown in panel a, the solar wind dynamic pressure was steady. The SYM-H index from -20 to -50 covered part of the main phase and the recovery phase in a moderate storm (see panel b). The AE index increased from 400 to $\sim$1000 at around 0510UT. The substorm around 0510UT is selected for analysis. Intuitively, intense solar wind and large geomagnetic storms may have more free energy to drive MeV electron injection events. However this event and similar events in previous studies indicate frequent occurrence of MeV electron injections during moderate activity, suggesting a complex chain of processes through

55455, USA

99 which MeV electron injections can drain free energy from the magnetosphere.

100

101 Figure 1d and 1e show the DC magnetic field and electric field from RBSP-A. The
102 magnetic field data are the 1s-resolution data from the EMFISIS fluxgate magnetometer
103 [*Kletzing et al.*, 2013]. The typical dipolarization signal is a rapid increase in **B**z that is
104 often associated with a decrease in **B**x. In Figure 1d, several dipolarizations with different
105 timescales can be clearly identified from about 0440UT to 0740UT. The spin-resolution
106 electric field from the EFW instrument [*Wygant et al.*, 2013] in the modified GSE coordi-
107 nates is shown in Figure 1e. **E**z and **E**y are in the spin plane and close to the GSE-z and
108 GSE-y within 20 degrees. In the regime of DC and ULF wave measurement, the electric
109 field component **E**x along the spin axis can be deduced from the **E**· **B**=0 assumption
110 if the angle between **B** and the spin plane is larger than 15 degrees [*Dai et al.*, 2013].
111 Electric field pulses of more than 20mV/m were frequently seen during dipolarizations on
112 this day. In particular, the duskward electric field was as large as 50mV/m during the
113 dipolarization around 0505UT.

114

115 Figure 1f, 1g and 1h show the electron and ion flux from the RBSP ECT [*Spence et al.*,
116 2013]. Panel f shows the electron differential flux from MagEIS [*Blake et al.*, 2013] in
117 the 31keV to 1.7MeV energy range . Electron of 10-100keV can increase by two orders
118 of magnitude during dipolarizations. Panel g shows the electron differential flux in the

---

[3]Department of Geophysics and Planetary

first three energy channels (1.8MeV, 2.1MeV and 2.6 MeV) from REPT [*Baker et al.*, 2013]. Figure 1h shows the differential flux of energetic ions from 69keV to 1.2MeV from MagEIS. In the substorm dipolarization near 0505UT, injected MeV ions were followed up by drift echos signals.

2.2. Dipolarization front and the dispersionless injection at RBSP

Figure 2a-h presents an expanded view of the substorm injection at RBSP-A from 0445UT to 0515UT. An abrupt increase from 100nT to 140nT in the northward magnetic component **B**z, usually referred to as a dipolarization front (DF) [*Nakamura et al.*, 2002; *Runov et al.*, 2009; *Ge et al.*, 2011; *Fu et al.*, 2011; *Hwang et al.*, 2011; *Zhou et al.*, 2014], is identified around 0506UT in panel b and marked by the gray bar. The DF, which lasted about 40s from 05:05:40UT to 05:06:20UT, was accompanied by an extremely large dawn-dusk electric field **E**y and a rapid increase in 30keV to 2.6MeV electrons. The dawn-dusk dipolarization electric field corresponded to a large earthward **E**$\times$ **B** in panel d. Even though it decelerates in the near-Earth region,a high-speed bursty bulk flow [*Angelopoulos et al.*, 1992] may occasionally penetrate deep into the inner magnetosphere. Because of the large **B**x in the inner magnetosphere, the DF was also related to a large **V**z ($\sim$ -**E**y/**B**x) toward the equatorial plane. In addition, **E**z corresponded to a flow deflected toward flanks at about 100km/s, likely due to the rising pressure in the inner magnetosphere.

Sciences, University of Science and

The electron injection of electrons at RBSP-A was dispersionless (Figure 2e,f). As shown in panel g and h, the pitch angle distribution (PAD) of injected MeV electrons was more concentrated around 90 degrees at the DF and thereafter spread out in a more isotropic distribution. The major acceleration mechanisms of electrons in dipolarizations, betatron acceleration and Fermi acceleration, are characterized by an energy increase associated with the perpendicular and parallel velocities, respectively [*Northrop*, 1963; *Birn et al.*, 2013; *Fu et al.*, 2011]. The PAD observations thus indicates that the acceleration of MeV electrons at the DF is mostly caused by betatron acceleration. Before the DF, energetic electrons appear to drop out due to the stretching of field lines. Behind the dipolarization front from 05:06:10UT to 05:07:10UT was the high **B**z region, usually referred to as the dipolarizing flux bundle (DFB) [*Liu et al.*, 2013]. The DFB was associated with an elevated flux of energetic electrons.

2.3. The dispersive injection at THEMIS-D

Figure 2i-k present the simultaneous observations form THEMIS-D from 0445UT to 0515UT in the predawn sector (MLT=4) at L$\sim$7. Because of the dipolarization's azimuthal localization, THEMIS-D did not observe the dipolarization signals. After 0506UT, THEMIS-D observed an increase in 720keV electrons fluxes followed by increases in lower-energy electron fluxes, usually referred to as a dispersed injection. Such dispersion signals result from the energy dependence of electron drift velocities after electrons are released simultaneously from an injection region [e.g.,*Reeves et al.* [1991]]. From the

Technology of China, PRC

timing difference of the initial flux increases, the injected electrons at THEMIS-D corresponded to a release of dispersionless electrons at ∼MLT=2-3 around 0505-0506UT.

2.4. Signals of MeV electron injection from LANL-GEO and GOES at geosynchronous altitude

The LANL-94 and LANL-97 spacecraft were at MLT∼1.8 and ∼6.5, respectively. Figure 2l,m show MeV electrons observations from these two spacecraft. LANL-94 was near the eastern edge of the injection region and LANL-97 was outside the injection region. Starting from 0502UT, LANL-94 observed an injection of MeV electrons. The onset time was close to that at GOES 13 shown in Figure 2o. Dispersed, drifting electron populations up to 3MeV, an unambiguous signature of MeV electron injections, were clearly seen by LANL-97 from 0506UT.

The GOES 13 and GOES 15 spacecraft were on the nightside, monitoring the injection at the geosynchronous altitude. Figure 2n-q show GOES 13 and GOES 15 observations of the magnetic fields and energetic particles. Starting from ∼0502UT, GOES 13, which was at the midnight within the injection region, observed a sustained dipolarization associated with injection of >0.6MeV and >2.0MeV electrons. The dipolarization at GOES 13 involved a increase of **B**z toward an elevated level. This type of dipolarization is usually thought of as a global dipolarization that is possibly related to but distinct from a

---

[4]Department of Physics and Astronomy,

dipolarization front [*Nakamura et al.*, 2011].

Based on the 2-3 minutes timing difference of the maximum electron flux increases at GOES 13 and RBSP-A, we obtain a 40-60 km/s earthward propagation velocity of the injection region from GOES 13 to RBSP-A. This slow earthward propagation of the injection region is consistent with those in previous statistical studies by *Moore et al.* [1981] and *Reeves et al.* [1996]. Similar to THEMIS-D, GOES 15 was located outside the injection region. Dipolarization signals were absent at GOES 15. From 0507UT-0508UT, the injection started to populate the electrons at the geosynchronous altitude. As a result, GOES 15 observed a persistent increase in >0.6MeV and >2.0MeV electron fluxes.

2.5. Increases of MeV electron PSD in the outer radiation belt

Several injections occurred between 05UT and 08UT on 26 April. Figure 3 presents the electron PSD as a function of the first and second adiabatic invariant from RBSP-A in the 5 hours before and after the injections. The electron PSD is plotted at the fixed second adiabatic invariant $K = 0.1 \pm 0.02$ $G^{1/2}$km and first adiabatic invariant $\mu = 1000 \pm 20, 1500 \pm 20, 2000 \pm 20$ MeV/G. The PSD is presented in the GEM (Geospace Environment Modeling) units $(c/MeV/cm)^3$ [*Chen et al.*, 2005]. The parameter K is evaluated based on the T04 models [*Tsyganenko and Sitnov*, 2005] and available from the Ephemeris data files on the RBSP ECT website. Note that there is uncertainty (10-20%) in K due to the inaccuracy of the magnetic field model near the injection region. This

University of Iowa, Iowa, IA 52245

magnitude of uncertainty in K is expected to produce very little difference in Figure 3. The selected set of μ and K approximately corresponds to 1-2 MeV electrons mirrored at low magnetic latitude at the geosynchronous altitude. Before the injections, the PSD at $\mu = 1000$MeV/G is 10^{-9}-10^{-8}(c/MeV/cm)^3 at L=4-5.5. After the injections, the electron PSD at $\mu = 1000$ MeV/G increased by an order of magnitude to 10^{-8}-10^{-7}(c/MeV/cm)^3 at L=4.8-5.6. The PSD of higher energy electrons at $\mu = 1500$MeV/G and $\mu = 2000$MeV/G increased by one order of magnitude as well. The increases of MeV electrons at L=4.8-5.7 were detected between 08UT and 09UT, indicating that the acceleration of MeV electrons was finished before 08UT, fewer than 3 hours after the injection. The 3-hour timescale is generally less than that characterized by whistler wave-driven acceleration ($\sim$10hours) or radial diffusion ($\sim$1day).

In the following, we examine if whistler wave-driven acceleration or radial diffusion can be responsible for the enhancement in Figure 3. We first estimate the wave power needed to produce the observed fast acceleration ($\sim$ 3 hours) by local wave acceleration. The timescale for the energization can be estimated as $1/(D_{EE}/E^2)$, where D_{EE} is the diffusion coefficient in the energy space and E is the energy of particles. D_{EE} is proportional to the wave power B_w^2 of the whistler waves. According to a previous whistler wave model by [*Horne et al.*, 2005], it took $\sim$20 hours for whistler waves with amplitude 50-100 pT to increase the flux of 1MeV electrons by one order of magnitude. In our event, the

[5]Laboratory for Atmospheric and Space

acceleration occurs within less than 3 hours. For wave-acceleration to be viable in this event, we need a continuous presence of strong whistler waves with amplitude >200pT. Assume a few hundred Hz bandwidth of the whistler waves, the required wave power is larger than $10^{-4}nT^2/Hz$. Figure 4 shows the observed wave power B_w^2 from RBSP-A and THEMIS-E. At the nightside, RBSP-A did not see the required strong whistler wave activity. Lower-band ($<0.5f_{ce}$) whistler waves are sparsely observed from 0520UT to 0600UT and 0730UT to 0840UT. The power of whistler waves was mostly less than $10^{-6}nT^2/Hz$, more than two orders of magnitude less than that of the whistler waves considered to effectively energize MeV electrons [*Su et al.*, 2014]. At the dawnside, THEMIS-D was at large L (L=6.7-9.8) from 05UT to 08UT; THEMIS-E encountered L=4-5.7 at dawn around 0630UT-0710UT and did not observe strong whistler waves (panel d of Figure 4). According to the statistical result *Li et al.* [2009], strong (>100 pT) whistler waves have a higher occurrence rate at nightside and dawnside. With an absence of continuous strong whistler waves at nightside (RBSP-A) and dawnside (THEMIS E) in this event, it is highly unlikely to have strong whistler waves at other locations during this 3 hour time period. Thus, we conclude that whistler wave-driven acceleration is unlikely to produce the electron enhancement in Figure 3.

Now we estimate whether radial diffusion is possible to produce the acceleration. How quickly radial diffusion can occur is proportional to the power of random wave fields in the ULF frequency band. ULF waves can be driven by solar wind or sources internal to

Physics, University of Colorado, Boulder,

237 the magnetosphere. Panel c and e of Figure 4 show the ULF power spectra from RBSP
238 and THEMIS for this event. At RBSP-A, most Fourier power from 05UT-08UT is due

CO 80303

[6]Space Sciences Department, The Aerospace Corporation, Los Angeles, CA 90009, USA

[7]Los Alamos National Laboratory, Los Alamos, NM, USA

[8]Department of Physics Institute for Earth, Oceans and Space, University of New Hampshire,Durham, New Hampshire 03824

[9]Department of Earth, Planetary and Space Sciences and Institute of Geophysics and Planetary Physics, University of California Los Angeles, Los Angeles, CA 90095, USA.

[10]Institute of Geophysics and extraterrestrial Physics, University of Braunschweig, Germany

[11]Department of Physics, University Of Texas, Dallas

to the zigzag shape of **B** in dipolarizations. A zigzag shape naturally corresponds to a broadband Fourier power spectrum. But these broadband power spectra are not random fluctuations which can lead to radial diffusion. Only around 06UT and 08UT, there were some ULF wave spectra ($10^2 - 10^3 nT^2/Hz$) that may cause radial diffusion. The ULF wave power observed by THEMIS-E is $10^1 - 10^2 nT^2/Hz$, one order magnitude smaller. The observed ULF wave spectra, which are comparable to or less than those in past statistic results [*Ozeke et al.*, 2012], are too weak and sporadic to cause fast radial diffusion in less than 3 hours in this event.

Based on the above estimates, whistler wave-driven acceleration and radial diffusion are unlikely responsible for the MeV electron enhancement in Figure 3. We conclude that substorm injection is primarily responsible for increases of MeV electrons at L >4.8 in this event. The PSD increase reflects a a high PSD of source populations that were directly transported to RBSP. The inferred source of high PSD may relate to a positive gradient of PSD in radial direction [e.g., *Turner et al.* [2010]] or a transient process.

2.6. Schematic: the dipolarization and injection of MeV electrons

The main dipolarization and injection observations are summarized in the schematic in Figure 4. Located at the nightside geosynchronous altitude, GOES 13 and LANL-94 first encountered the injection region at around 0502UT. The dipolarization at GOES 13 was a large-scale dipolarization in which **B**z and energetic electron fluxes increase to an elevated level. At 0506UT, RBSP-A observed a small-scale dipolarization front. From

the timing difference (3-4 minutes) of the dispersionless injection at GOES 13 and RBSP-A, the injection region propagated earthward at 30-40 km/s, consistent with previous statistic studies [*Moore et al.*, 1981; *Reeves et al.*, 1996]. The different characteristics of dipolarizations at these two spacecraft reflect a strong inhomogeneity of the injection region across the azimuthal direction and/or the radial direction. The observation of this event suggests a patchy , rapidly varying injection region.

As the injection region propagated earthward inside the geosynchronous altitude, the dipolarization electric field presumably was reduced at L=6.8. Gradient **B** drift gradually became dominant and particles started to drift away from the injection region. By 0506UT when the injection region reached RBSP, large amounts of energetic electrons were released from the injection region. Outside the injection region, LANL-97 observed dispersed and drifting MeV electrons; THEMIS observed the energy-dispersive drifting electrons >700keV and GOES 15 observed slow MeV electrons increases. Based on the PSD results in Figure 3, the injection region may penetrate to L=4.8.

3. Summary and Discussion

We present observations of an MeV electron injection event measured by RBSP at L=5.5 and THEMIS, LANL-GEO and GOES at geosynchronous altitude. This MeV electron injection event is particularly interesting because it featured a large (50mV/m) duskward electric field pulse associated with a dipolarization front at RBSP-A. Pitch angle observations indicated that betatron acceleration of the MeV electrons was operating

at the dipolarization front. Dispersed, drifting MeV electrons were observed at LANL-GEO. Corresponding signals of MeV electron injection were also observed by GOES and THEMIS at the geosynchronous altitude. The injection region propagated earthward at a speed of 30-40km/s inside the geosynchronous altitude. After a series of injections, the PSD of MeV electrons increased by a order of magnitude at L>4.8 in less than 3 hours. We show evidence that whistler wave-driven acceleration and radial diffusion are unlikely responsible for the MeV electron enhancement in this event. Our observations indicate that the deep injection associated with strong dipolarization electric fields can supply significant MeV electrons to the outer radiation belt.

Substorm injection can be thought of as a coherent radial transport process. The electric field must be intense and nonrandom during its interaction with particles for such coherent radial transport to be effective. (A 1-10s MeV electron injection caused by shock-induced electric fields is an example of coherent transport [*Blake et al.*, 1992; *Li et al.*, 1993; *Wygant et al.*, 1994].) The intensity and structure of dipolarization electric fields may be important in differentiating injections of MeV electrons from injections of sub-relativistic electrons. The large magnitude of the dipolarization electric field ($\sim$50mV/m) in this event far exceeded the values (several mV/m) used in most injection models. Regarding the electric field structure, our observations suggested that the injection region (and probably the dipolarization electric field) is likely to be patchy and/or rapidly-varying. These observations may shed lights on future efforts to model injections of MeV electrons.

Another important factor in MeV electron injections is the source population. During near-Earth injections, energetic electrons are transported earthward and trapped in the inner magnetosphere. The increase of PSD in Figure 3 reflects a high PSD of the source populations that were directly transported to the outer radiation belt. The high PSD of the source population needed for MeV electron injection may be from the high energy tail of the plasma sheet populations, a temporal source in the magnetotail (e.g., reconnection) or accumulated from previous substorms.

Acknowledgments. This work was supported by NNSFC grant 41231067 and in part by the Specialized Research Fund for State Key Laboratories of China. Work at UMN was supported by a contract from APL for the development of RBSP/EFW. EMFISIS is supported by a JHU/APL contract 921647. L.C. would like to acknowledge the support of the NASA grant NNX15AF55G. DLT, GDR, and XL are thankful for support from the International Space Science Institute's (ISSI) International Teams program. L.D. greatly appreciate Judy Hohl from UCLA for editorial help. The RBSP EMFISIS data is available at http://emfisis.physics.uiowa.edu/Flight/. The RBSP EFW data is available at http://rbsp.space.umn.edu/data/rbsp/. The RBSP ECT data is available at http://www.rbsp-ect.lanl.gov/. THEMIS data is available at http://themis.ssl.berkeley.edu/data/themis/. LANL-GEO data is provided by Geoffrey D. Reeves. GOES data is available at http://satdat.ngdc.noaa.gov/sem/goes/data/. The OMNI data is available at CDAWeb. The SYM-H data are provided by the World Data

Center for Geomagnetism, Kyoto.

References

Angelopoulos, V., W. Baumjohann, C. F. Kennel, F. V. Coronti, M. G. Kivelson, R. Pellat, R. J. Walker, H. Luehr, and G. Paschmann (1992), Bursty bulk flows in the inner central plasma sheet, *J. Geophys. Res.,* , *97*, 4027–4039, doi:10.1029/91JA02701.

Ashour-Abdalla, M., M. El-Alaoui, M. L. Goldstein, M. Zhou, D. Schriver, R. Richard, R. Walker, M. G. Kivelson, and K.-J. Hwang (2011), Observations and simulations of non-local acceleration of electrons in magnetotail magnetic reconnection events, *Nature Physics*, *7*, 360–365, doi:10.1038/nphys1903.

Baker, D. N., T. I. Pulkkinen, V. Angelopoulos, W. Baumjohann, and R. L. McPherron (1996), Neutral line model of substorms: Past results and present view, *J. Geophys. Res.,* , *101*, 12,975–13,010, doi:10.1029/95JA03753.

Baker, D. N., et al. (2013), The Relativistic Electron-Proton Telescope (REPT) Instrument on Board the Radiation Belt Storm Probes (RBSP) Spacecraft: Characterization of Earth's Radiation Belt High-Energy Particle Populations, *Space Science Reviews*, *179*, 337–381, doi:10.1007/s11214-012-9950-9.

Birn, J., M. F. Thomsen, J. E. Borovsky, G. D. Reeves, D. J. McComas, R. D. Belian, and M. Hesse (1998), Substorm electron injections: Geosynchronous observations and test particle simulations, *J. Geophys. Res.*, *103*, 9235–9248, doi:10.1029/97JA02635.

Birn, J., M. Hesse, R. Nakamura, and S. Zaharia (2013), Particle acceleration in dipolarization events, *Journal of Geophysical Research (Space Physics)*, *118*, 1960–1971,

345 doi:10.1002/jgra.50132.

346 Blake, J., et al. (2013), The magnetic electron ion spectrometer (mageis) instruments
347 aboard the radiation belt storm probes (rbsp) spacecraft, *Space Science Reviews*, pp.
348 1–39, doi:10.1007/s11214-013-9991-8.

349 Blake, J. B., W. A. Kolasinski, R. W. Fillius, and E. G. Mullen (1992), Injection of
350 electrons and protons with energies of tens of MeV into L less than 3 on 24 March 1991,
351 *Geophys. Res. Lett.,* , *19*, 821–824, doi:10.1029/92GL00624.

352 Cattell, C. A., and F. S. Mozer (1984), Substorm Electric Fields in the Earth's Magneto-
353 tail, in *Magnetic Reconnection in Space and Laboratory Plasmas*, edited by E. W. Hones
354 Jr., pp. 208–215.

355 Chen, Y., R. H. W. Friedel, G. D. Reeves, T. G. Onsager, and M. F. Thomsen (2005),
356 Multisatellite determination of the relativistic electron phase space density at geosyn-
357 chronous orbit: Methodology and results during geomagnetically quiet times, *Journal*
358 *of Geophysical Research (Space Physics)*, *110*, A10210, doi:10.1029/2004JA010895.

359 Dai, L., et al. (2013), Excitation of poloidal standing Alfvén waves through drift resonance
360 wave-particle interaction, *Geophys. Res. Lett.,* , *40*, 4127–4132, doi:10.1002/grl.50800.

361 Dai, L., et al. (2014), Evidence for injection of relativistic electrons into the Earth's outer
362 radiation belt via intense substorm electric fields, *Geophys. Res. Lett.,* , *41*, 1133–1141,
363 doi:10.1002/2014GL059228.

364 Fairfield, D. H., et al. (1998), Geotail observations of substorm onset in the inner magne-
365 totail, *J. Geophys. Res.*, *103*, 103–118, doi:10.1029/97JA02043.

366 Fok, M.-C., T. E. Moore, and W. N. Spjeldvik (2001), Rapid enhancement of radiation
367 belt electron fluxes due to substorm dipolarization of the geomagnetic field, *J. Geophys.*
368 *Res.*, *106*, 3873–3882, doi:10.1029/2000JA000150.

369 Fok, M.-C., T. E. Moore, P. C. Brandt, D. C. Delcourt, S. P. Slinker, and J. A. Fedder
370 (2006), Impulsive enhancements of oxygen ions during substorms, *Journal of Geophys-*
371 *ical Research (Space Physics)*, *111*, A10222, doi:10.1029/2006JA011839.

372 Friedel, R. H. W., A. Korth, and G. Kremser (1996), Substorm onsets observed by CRRES:
373 Determination of energetic particle source regions, *J. Geophys. Res.*, *101*, 13,137–13,154,
374 doi:10.1029/96JA00399.

375 Fu, H. S., Y. V. Khotyaintsev, M. André, and A. Vaivads (2011), Fermi and betatron
376 acceleration of suprathermal electrons behind dipolarization fronts, *Geophys. Res. Lett.,*
377 , *38*, L16104, doi:10.1029/2011GL048528.

378 Gabrielse, C., V. Angelopoulos, A. Runov, and D. L. Turner (2012), The effects of
379 transient, localized electric fields on equatorial electron acceleration and transport to-
380 ward the inner magnetosphere, *Journal of Geophysical Research (Space Physics)*, *117*,
381 A10213, doi:10.1029/2012JA017873.

382 Ge, Y. S., J. Raeder, V. Angelopoulos, M. L. Gilson, and A. Runov (2011), Interaction of
383 dipolarization fronts within multiple bursty bulk flows in global MHD simulations of a
384 substorm on 27 February 2009, *Journal of Geophysical Research (Space Physics)*, *116*,
385 A00I23, doi:10.1029/2010JA015758.

386 Glocer, A., M.-C. Fok, T. Nagai, G. Tóth, T. Guild, and J. Blake (2011), Rapid rebuild-
387 ing of the outer radiation belt, *Journal of Geophysical Research (Space Physics)*, *116*,

A09213, doi:10.1029/2011JA016516.

Horne, R. B., R. M. Thorne, S. A. Glauert, J. M. Albert, N. P. Meredith, and R. R. Anderson (2005), Timescale for radiation belt electron acceleration by whistler mode chorus waves, *Journal of Geophysical Research (Space Physics)*, *110*, A03225, doi:10.1029/2004JA010811.

Hwang, K.-J., M. L. Goldstein, E. Lee, and J. S. Pickett (2011), Cluster observations of multiple dipolarization fronts, *Journal of Geophysical Research (Space Physics)*, *116*, A00I32, doi:10.1029/2010JA015742.

Ingraham, J. C., T. E. Cayton, R. D. Belian, R. A. Christensen, R. H. W. Friedel, M. M. Meier, G. D. Reeves, and M. Tuszewski (2001), Substorm injection of relativistic electrons to geosynchronous orbit during the great magnetic storm of March 24, 1991, *J. Geophys. Res.*, *106*, 25,759–25,776, doi:10.1029/2000JA000458.

Kim, H.-J., A. A. Chan, R. A. Wolf, and J. Birn (2000), Can substorms produce relativistic outer belt electrons?, *J. Geophys. Res.*, *105*, 7721–7736, doi:10.1029/1999JA900465.

Kletzing, C., et al. (2013), The electric and magnetic field instrument suite and integrated science (emfisis) on rbsp, *Space Science Reviews*, pp. 1–55, doi:10.1007/s11214-013-9993-6.

Li, W., et al. (2009), Global distribution of whistler-mode chorus waves observed on the THEMIS spacecraft, *Geophys. Res. Lett.,* , *36*, L09104, doi:10.1029/2009GL037595.

Li, X., I. Roth, M. Temerin, J. R. Wygant, M. K. Hudson, and J. B. Blake (1993), Simulation of the prompt energization and transport of radiation belt particles during the March 24, 1991 SSC, *Geophys. Res. Lett.*, *20*, 2423–2426, doi:10.1029/93GL02701.

Li, X., D. N. Baker, M. Temerin, G. D. Reeves, and R. D. Belian (1998), Simulation of dispersionless injections and drift echoes of energetic electrons associated with substorms, *Geophys. Res. Lett.*, *25*, 3763–3766, doi:10.1029/1998GL900001.

Li, X., T. E. Sarris, D. N. Baker, W. K. Peterson, and H. J. Singer (2003), Simulation of energetic particle injections associated with a substorm on August 27, 2001, *Geophys. Res. Lett.*, *30*(1), 1004, doi:10.1029/2002GL015967.

Liu, J., V. Angelopoulos, A. Runov, and X.-Z. Zhou (2013), On the current sheets surrounding dipolarizing flux bundles in the magnetotail: The case for wedgelets, *Journal of Geophysical Research (Space Physics)*, *118*, 2000–2020, doi:10.1002/jgra.50092.

Liu, W. L., et al. (2009), Observation and modeling of the injection observed by THEMIS and LANL satellites during the 23 March 2007 substorm event, *Journal of Geophysical Research (Space Physics)*, *114*, A00C18, doi:10.1029/2008JA013498.

Mauk, B. H., N. J. Fox, S. G. Kanekal, R. L. Kessel, D. G. Sibeck, and A. Ukhorskiy (2012), Science Objectives and Rationale for the Radiation Belt Storm Probes Mission, *Space Science Reviews*, doi:10.1007/s11214-012-9908-y.

Moore, T. E., R. L. Arnoldy, J. Feynman, and D. A. Hardy (1981), Propagating substorm injection fronts, *J. Geophys. Res.,* , *86*, 6713–6726, doi:10.1029/JA086iA08p06713.

Nagai, T., A. S. Yukimatu, A. Matsuoka, K. T. Asai, J. C. Green, T. G. Onsager, and H. J. Singer (2006), Timescales of relativistic electron enhancements in the slot region, *Journal of Geophysical Research (Space Physics)*, *111*, A11205, doi:10.1029/2006JA011837.

Nakamura, R., et al. (2002), Motion of the dipolarization front during a flow burst event observed by Cluster, *Geophys. Res. Lett.,* , *29*, 1942, doi:10.1029/2002GL015763.

Nakamura, R., et al. (2011), Flux transport, dipolarization, and current sheet evolution during a double-onset substorm, *Journal of Geophysical Research (Space Physics)*, *116*, A00I36, doi:10.1029/2010JA015865.

Northrop, T. G. (1963), Adiabatic Charged-Particle Motion, *Reviews of Geophysics and Space Physics*, *1*, 283–304.

Ozeke, L. G., I. R. Mann, K. R. Murphy, I. J. Rae, D. K. Milling, S. R. Elkington, A. A. Chan, and H. J. Singer (2012), ULF wave derived radiation belt radial diffusion coefficients, *Journal of Geophysical Research (Space Physics)*, *117*, A04222, doi:10.1029/2011JA017463.

Reeves, G. D., R. D. Belian, and T. A. Fritz (1991), Numerical tracing of energetic particle drifts in a model magnetosphere, *J. Geophys. Res.,* , *96*, 13,997, doi:10.1029/91JA01161.

Reeves, G. D., M. G. Henderson, P. S. McLachlan, R. D. Belian, R. H. W. Friedel, and A. Korth (1996), Radial propagation of substorm injections, in *International Conference on Substorms*, *ESA Special Publication*, vol. 389, edited by E. J. Rolfe and B. Kaldeich, p. 579.

Rowland, D. (2002), The Electrodynamics of the Inner Magnetosphere During Major Geoagnetic Storms, Ph.D. thesis, UNIVERSITY OF MINNESOTA.

Runov, A., V. Angelopoulos, M. I. Sitnov, V. A. Sergeev, J. Bonnell, J. P. McFadden, D. Larson, K.-H. Glassmeier, and U. Auster (2009), THEMIS observations of an earthward-propagating dipolarization front, *Geophys. Res. Lett.*, *36*, L14106, doi:10.1029/2009GL038980.

453 Sarris, T. E., X. Li, N. Tsaggas, and N. Paschalidis (2002), Modeling energetic particle in-
454 jections in dynamic pulse fields with varying propagation speeds, *Journal of Geophysical*
455 *Research (Space Physics)*, *107*, 1033, doi:10.1029/2001JA900166.

456 Sergeev, V. A., M. A. Shukhtina, R. Rasinkangas, A. Korth, G. D. Reeves, H. J. Singer,
457 M. F. Thomsen, and L. I. Vagina (1998), Event study of deep energetic particle injections
458 during substorm, *J. Geophys. Res.,* , *103*, 9217–9234, doi:10.1029/97JA03686.

459 Spence, H. E., et al. (2013), Science Goals and Overview of the Radiation Belt Storm
460 Probes (RBSP) Energetic Particle, Composition, and Thermal Plasma (ECT) Suite
461 on NASA's Van Allen Probes Mission, *Space Science Reviews*, *179*, 311–336, doi:
462 10.1007/s11214-013-0007-5.

463 Su, Z., et al. (2014), Quantifying the relative contributions of substorm injections and
464 chorus waves to the rapid outward extension of electron radiation belt, *Journal of*
465 *Geophysical Research (Space Physics)*, *119*, 10,023, doi:10.1002/2014JA020709.

466 Tsyganenko, N. A., and M. I. Sitnov (2005), Modeling the dynamics of the inner mag-
467 netosphere during strong geomagnetic storms, *Journal of Geophysical Research (Space*
468 *Physics)*, *110*, A03208, doi:10.1029/2004JA010798.

469 Tu, J.-N., K. Tsuruda, H. Hayakawa, A. Matsuoka, T. Mukai, I. Nagano, and S. Yag-
470 itani (2000), Statistical nature of impulsive electric fields associated with fast ion
471 flow in the near-Earth plasma sheet, *J. Geophys. Res.*, *105*, 18,901–18,908, doi:
472 10.1029/1999JA000428.

473 Turner, D., et al. (2015), Energetic electron injections deep into the inner magnetosphere
474 associated with substorm activity, *Geophysical Research Letters*.

Turner, D. L., X. Li, G. D. Reeves, and H. J. Singer (2010), On phase space density radial gradients of Earth's outer-belt electrons prior to sudden solar wind pressure enhancements: Results from distinctive events and a superposed epoch analysis, *Journal of Geophysical Research (Space Physics)*, *115*, A01205, doi:10.1029/2009JA014423.

Wygant, J., F. Mozer, M. Temerin, J. Blake, N. Maynard, H. Singer, and M. Smiddy (1994), Large amplitude electric and magnetic field signatures in the inner magnetosphere during injection of 15 MeV electron drift echoes, *Geophys. Res. Lett.*, *21*, 1739–1742, doi:10.1029/94GL00375.

Wygant, J. R., et al. (2013), The Electric Field and Waves Instruments on the Radiation Belt Storm Probes Mission, *Space Science Reviews*, *179*, 183–220, doi:10.1007/s11214-013-0013-7.

Yang, J., F. R. Toffoletto, R. A. Wolf, and S. Sazykin (2011), RCM-E simulation of ion acceleration during an idealized plasma sheet bubble injection, *Journal of Geophysical Research (Space Physics)*, *116*, A05207, doi:10.1029/2010JA016346.

Zaharia, S., J. Birn, R. H. W. Friedel, G. D. Reeves, M. F. Thomsen, and C. Z. Cheng (2004), Substorm injection modeling with nondipolar, time-dependent background field, *Journal of Geophysical Research (Space Physics)*, *109*, A10211, doi:10.1029/2004JA010464.

Zhang, J.-C., R. A. Wolf, R. W. Spiro, G. M. Erickson, S. Sazykin, F. R. Toffoletto, and J. Yang (2009), Rice Convection Model simulation of the substorm-associated injection of an observed plasma bubble into the inner magnetosphere: 2. Simulation results, *Journal of Geophysical Research (Space Physics)*, *114*, A08219, doi:10.1029/2009JA014131.

497 Zhou, X.-Z., V. Angelopoulos, J. Liu, A. Runov, and S.-S. Li (2014), On the origin of pres-
498 sure and magnetic perturbations ahead of dipolarization fronts, *Journal of Geophysical*
499 *Research (Space Physics)*, *119*, 211–220, doi:10.1002/2013JA019394.

Figure 1. Overview of solar wind conditions, the geomagnetic activity and RBSP-A observations on April 26, 2013. a) One-minute OMIN data of the solar wind dynamic pressure. b) The SYM-H index. c) AE index. d) 1s-resolution **B**x and **B**z components in GSM from RBSP-A. e) Spin-fit **E**y and **E**z in MGSE from RBSP-A. f) The different flux of energetic electrons from MagEIS onboard RBSP-A. g) The different flux of energetic electrons from REPT onboard RBSP-A. h) The different flux of energetic ions from MagEIS onboard RBSP-A.

Figure 2. The 20-minute expanded view of the injection event from 0445UT to 0515UT. Panels from a) to h) are RBSP-A measurements of a) the magnitude of **B**,b)**B**x and **B**z in GSM, c) the spin-fit electric field in GSM (the spin-axis electric field is obtained from the **E**·**B**=0 assumption), d) the **E** ×**B** drift velocity in GSM, e) fluxes of energetic electrons from MagEIS, f) fluxes of energetic electrons from REPT, g) PAD of 0.9MeV electrons from MagEIS, h) PAD of 1.8MeV electrons from REPT. Panels from i) to k) are THEMIS-D measurements of i) the spin-resolution magnetic field in GSM, h) the spin-resolution electric field in GSM, k) differential energy fluxes of energetic electrons from SST. Panels l) and m) are counts per second of MeV electrons (averaged over 20s) measured from LANL-94 and LANL-94, respectively. Panels n) and o) are GOES 13 measurements of three magnetic field components in GSM and the integral flux of energetic electrons. Panels p) and q) are GOES 15 measurements of three magnetic field components in GSM and the integral flux of energetic electrons.

Figure 3. The electron PSD at fixed K and μ before the injections (left panel) and after the injections (right panel).

Figure 4. The observations of wave power spectra from RBSP-A and THEMIS-E. a) and b), RBSP-A observations of the wave power spectra (10-10^4 Hz) of one electric field component (**E**12) and one magnetic field component (**B**w) from EFW burst data in VLF frequency range. Form top to the bottom, the three horizontal black lines in each panel represent the local electron gyro-frequency (f_{ce}), half f_{ce} and the lower hybrid frequency. c) RBSP-A observations of the power spectra in the ULF frequency band. d) and e), THEMIS-E observations of wave power spectra in the VLF frequency and ULF frequency band. The black region in e) is the inner radiation belt with strong Dc magnetic fields.

Figure 5. The xy-plane schematic of RBSP-A, LANL-94, LANL-97, THEMIS-D, GOES 13 and GOES 15 during the dipolarization and injection of MeV electrons.

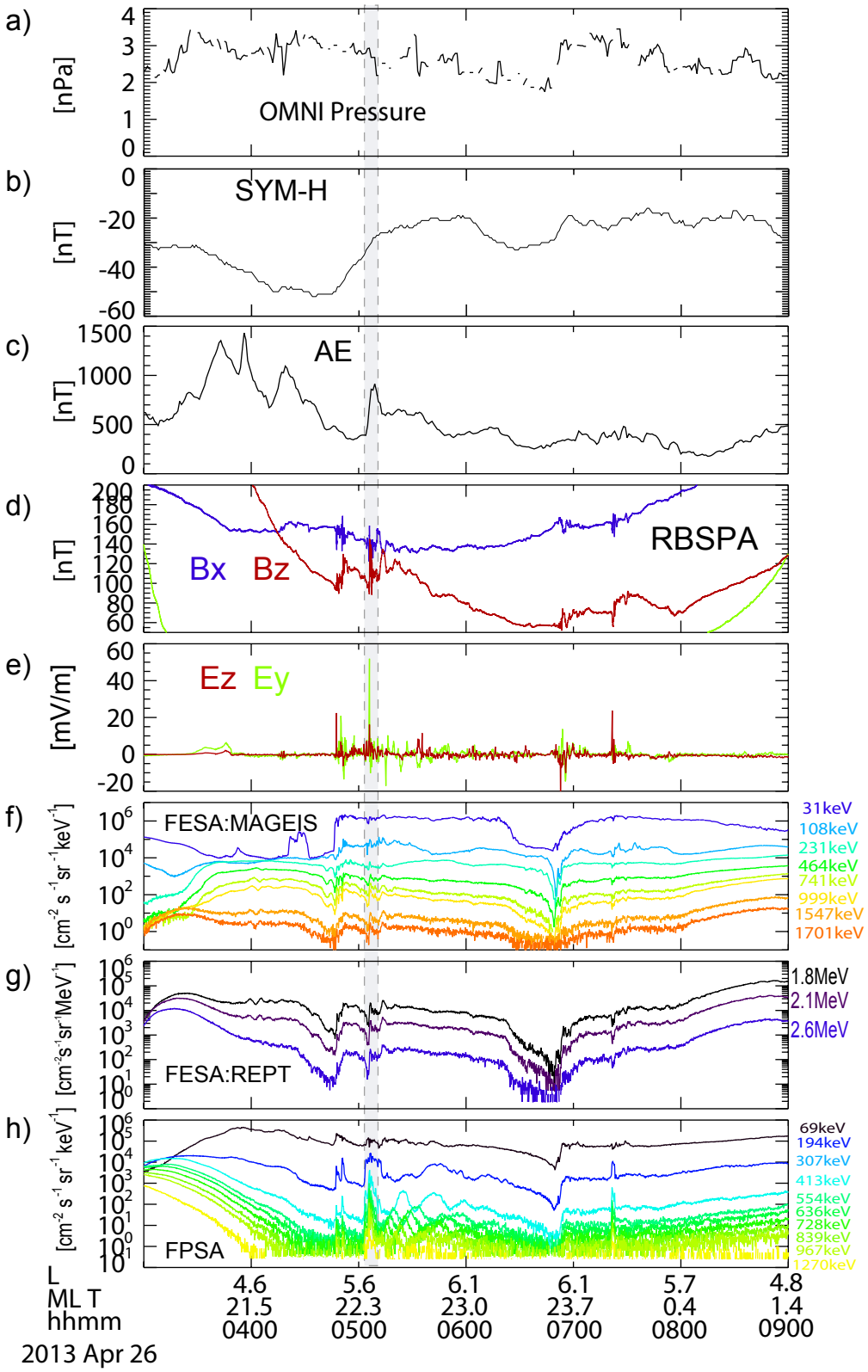
a)
[nPa]
OMNI Pressure
b)
SYM-H
[nT]
c)
AE
[nT]
d)
[nT]
Bx
Bz
RBSPA
e)
[mV/m]
Ez
Ey
f)
FESA:MAGEIS
[cm-2 s-1 sr-1 keV-1]
31keV
108keV
231keV
464keV
741keV
999keV
1547keV
1701keV
g)
[cm-2 s-1 sr-1 MeV-1]
FESA:REPT
1.8MeV
2.1MeV
2.6MeV
h)
[cm-2 s-1 sr-1 keV-1]
FPSA
69keV
194keV
307keV
413keV
554keV
636keV
728keV
839keV
967keV
1270keV
L
ML T
hhmm
4.6
21.5
0400
5.6
22.3
0500
6.1
23.0
0600
6.1
23.7
0700
5.7
0.4
0800
4.8
1.4
0900
2013 Apr 26

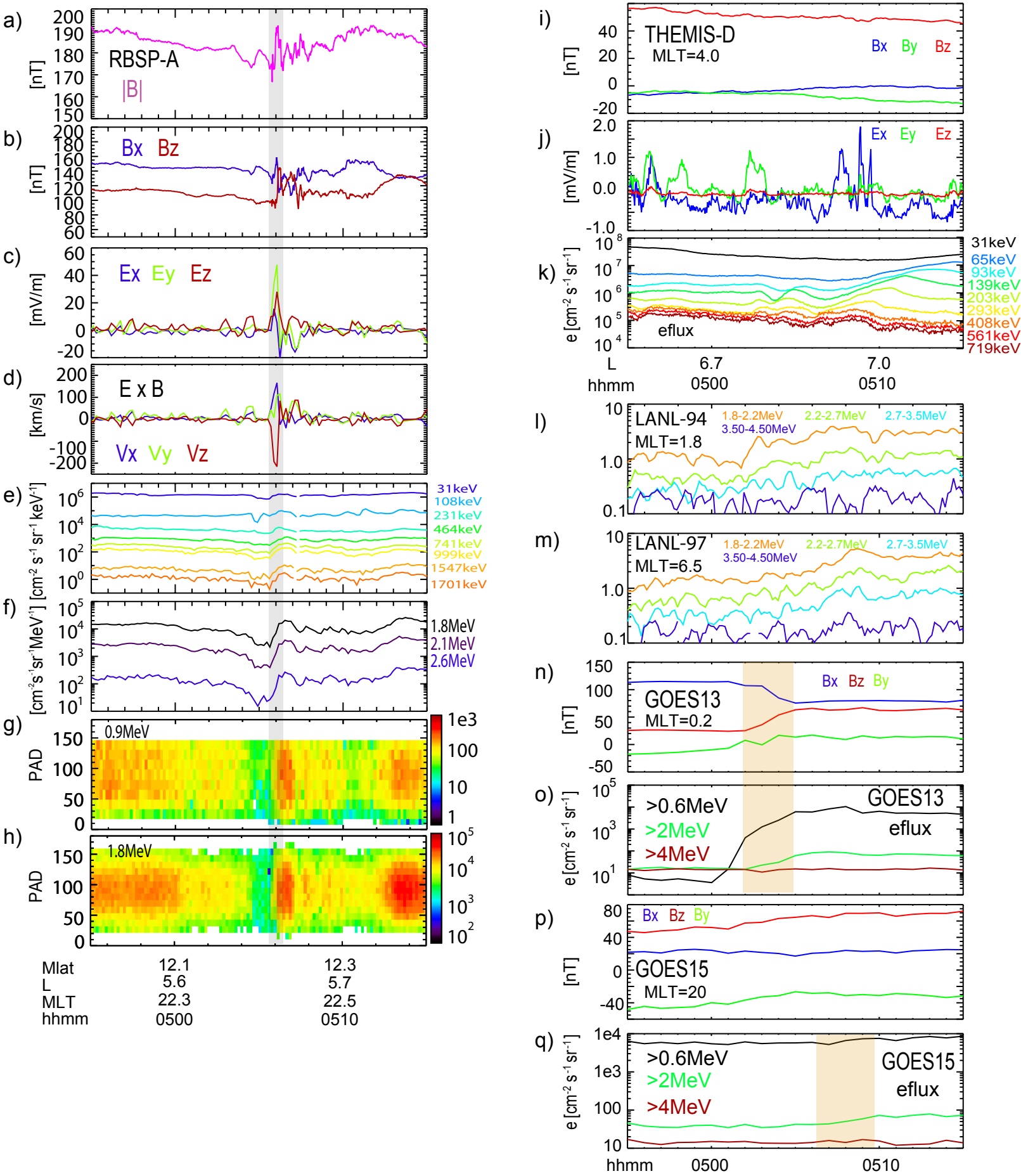
a)
RBSP-A
|B|
[nT]
b)
Bx Bz
[nT]
c)
Ex Ey Ez
[mV/m]
d)
E x B
Vx Vy Vz
[km/s]
e)
31keV
108keV
231keV
464keV
741keV
999keV
1547keV
1701keV
[cm-2 s-1 sr-1 keV-1]
f)
1.8MeV
2.1MeV
2.6MeV
[cm-2s-1sr-1MeV-1]
g)
0.9MeV
PAD
h)
1.8MeV
PAD
Mlat 12.1 12.3
L 5.6 5.7
MLT 22.3 22.5
hhmm 0500 0510
i)
THEMIS-D
MLT=4.0
Bx By Bz
[nT]
j)
Ex Ey Ez
[mV/m]
k)
31keV
65keV
93keV
139keV
203keV
293keV
408keV
561keV
719keV
eflux
e [cm-2 s-1 sr-1]
L 6.7 7.0
hhmm 0500 0510
l)
LANL-94
MLT=1.8
1.8-2.2MeV
2.2-2.7MeV
2.7-3.5MeV
3.50-4.50MeV
m)
LANL-97
MLT=6.5
n)
GOES13
MLT=0.2
Bx Bz By
[nT]
o)
>0.6MeV
>2MeV
>4MeV
GOES13
eflux
e [cm-2 s-1 sr-1]
p)
GOES15
MLT=20
Bx Bz By
[nT]
q)
>0.6MeV
>2MeV
>4MeV
GOES15
eflux
e [cm-2 s-1 sr-1]
hhmm 0500 0510

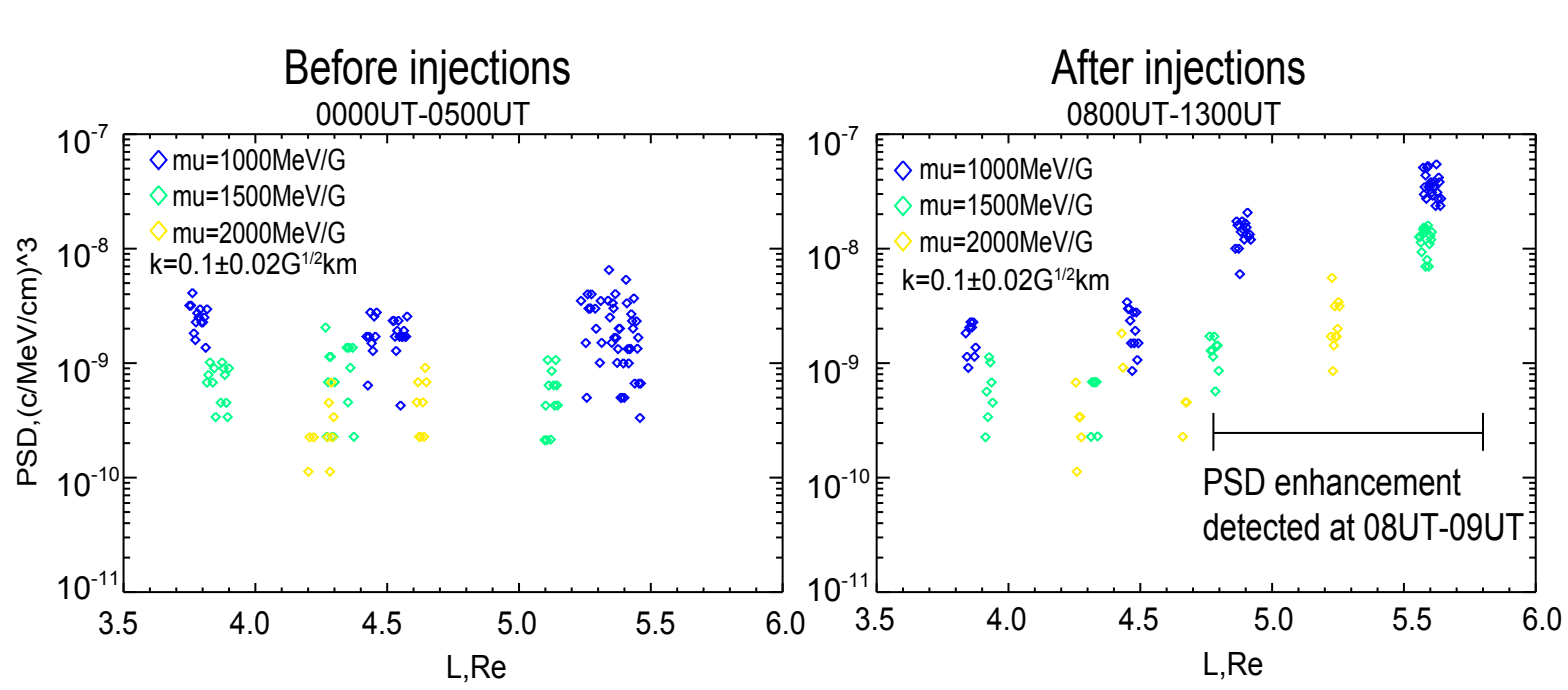
Before injections
0000UT-0500UT
After injections
0800UT-1300UT
mu=1000MeV/G
mu=1500MeV/G
mu=2000MeV/G
k=0.1±0.02G^1/2km
PSD,(c/MeV/cm)^3
L,Re
PSD enhancement
detected at 08UT-09UT

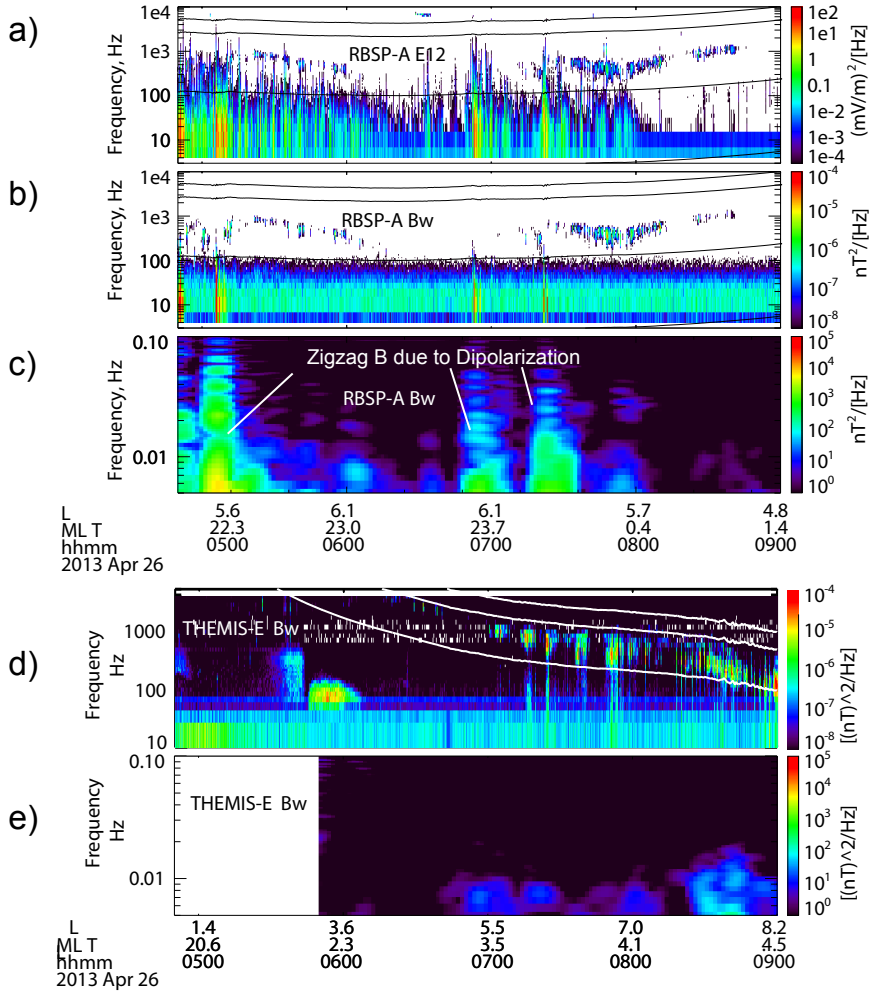
a)
b)
c)
d)
e)
RBSP-A E12
RBSP-A Bw
Zigzag B due to Dipolarization
RBSP-A Bw
THEMIS-E Bw
THEMIS-E Bw
Frequency, Hz
Frequency
Hz
1e4
1e3
100
10
0.10
0.01
1000
1e2
1e1
1
0.1
1e-2
1e-3
1e-4
(mV/m)^2/[Hz]
nT^2/[Hz]
[(nT)^2/Hz]
L
MLT
hhmm
2013 Apr 26
5.6
22.3
0500
6.1
23.0
0600
6.1
23.7
0700
5.7
0.4
0800
4.8
1.4
0900
1.4
20.6
0500
3.6
2.3
0600
5.5
3.5
0700
7.0
4.1
0800
8.2
4.5
0900

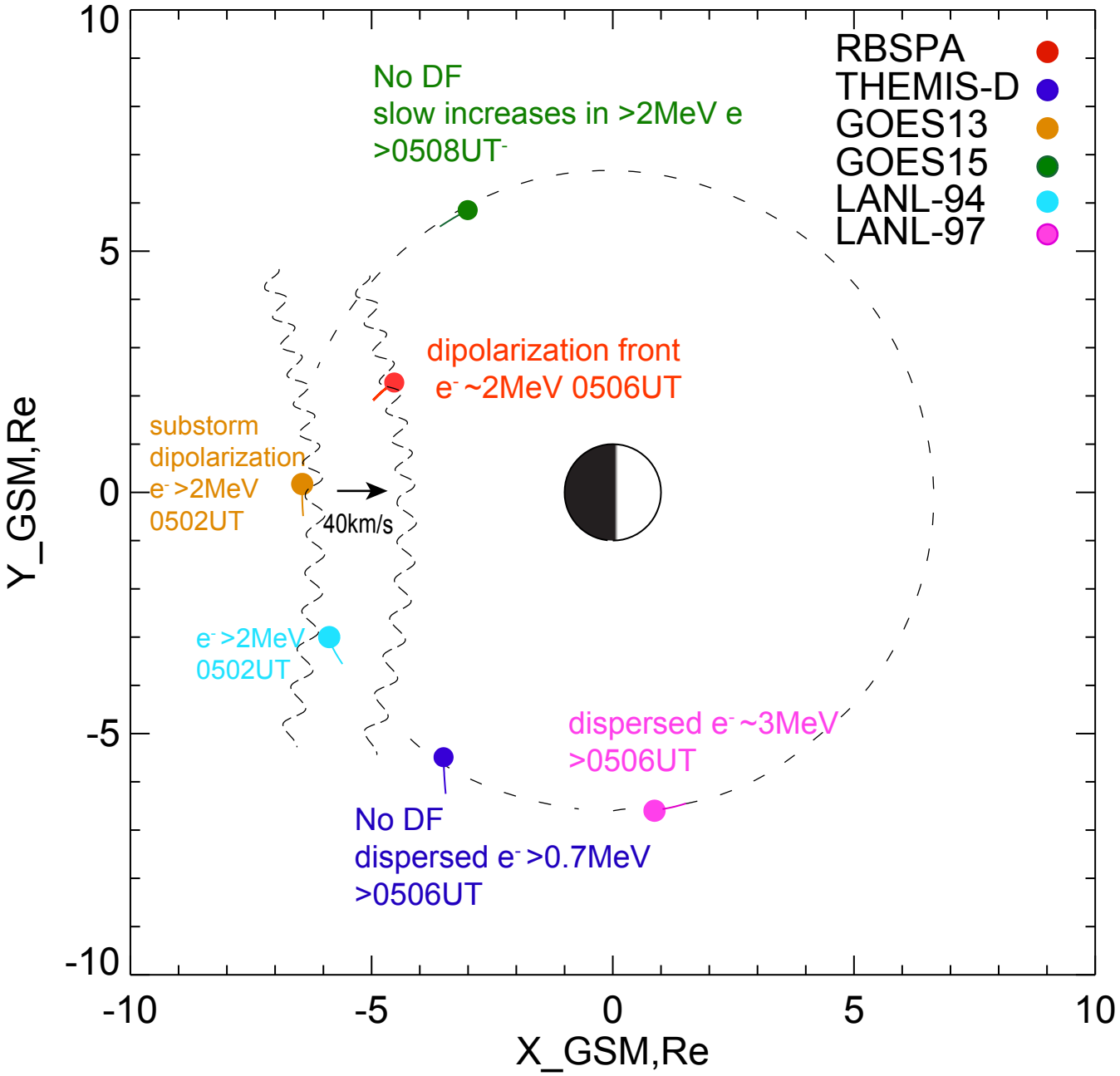
RBSPA
THEMIS-D
GOES13
GOES15
LANL-94
LANL-97
No DF
slow increases in >2MeV e
>0508UT-
dipolarization front
e- ~2MeV 0506UT
substorm
dipolarization
e- >2MeV
0502UT
40km/s
e- >2MeV
0502UT
dispersed e- ~3MeV
>0506UT
No DF
dispersed e- >0.7MeV
>0506UT
10
5
0
-5
-10
-10
-5
0
5
10
Y_GSM,Re
X_GSM,Re